Excitonic complexes in natural InAs/GaAs quantum dots

M. Zieliński,[1,*] K. Gołasa,[2,†] M. R. Molas,[2,3] M. Goryca,[2] T. Kazimierczuk,[2] T. Smoleński,[2] A. Golnik,[2] P. Kossacki,[2] A. A. L. Nicolet,[3] M. Potemski,[3] Z. R. Wasilewski,[4] and A. Babiński[2]

[1]*Institute of Physics, Faculty of Physics, Astronomy and Informatics, Nicolaus Copernicus University, Grudziadzka 5, 87-100 Torun, Poland*

[2]*Faculty of Physics, University of Warsaw, Pasteura 5, 02-093 Warszawa, Poland*

[3]*Laboratoire National des Champs Magnétiques Intenses, CNRS-UJF-UPS-INSA, 25, avenue des Martyrs, 38042 Grenoble, France*

[4]*Waterloo Institute for Nanotechnology, University of Waterloo 200 University Avenue West, Waterloo, Ontario, Canada N2L 3G1*

(Received 17 April 2014; revised manuscript received 20 January 2015; published 6 February 2015)

The quantum confinement in a typical quantum dot (QD) is determined primarily by the nanosystem's dimensions and average composition. We demonstrate, however, that excitonic properties of natural QDs formed in the InAs/GaAs wetting layer are governed predominantly by effects of random fluctuations of the lattice composition. It is shown that the biexciton binding energy is a very sensitive function of the lattice randomness with a nearly flat dependence on the exciton energy. The large variation in different random realizations of a QD structure is shown to lead in some cases to the reversal of the order of excitonic lines. Results of theoretical calculations correspond to statistical properties of neutral excitons and biexcitons as well as trions confined to single natural QDs studied in our microspectroscopic measurements. We observe substantial variation of the biexciton and trion binding energies as well as a correlation of the trion and the biexciton energies. The transition from the negative to the positive binding energy of the trion is also observed, which strongly supports the attribution of the observed trion to the positively charged exciton.

DOI: 10.1103/PhysRevB.91.085303 PACS number(s): 78.67.Hc, 73.21.La, 78.55.Cr

I. INTRODUCTION

Quantum confinement of carriers in semiconductor quantum dots (QDs) leads to numerous effects of fundamental character. This makes them objects of intense study (for a review, see Ref. [1]). The research is driven by both scientific curiosity and promising optoelectronic applications, e.g., optical quantum devices based on single-photon emission. One of the problems to be solved in order to use QDs in such applications is the statistical character of QDs in the structures which results in an inhomogeneous broadening of their emission energies. The emission energy depends on a confining potential, which in turn is a complicated function of the QD size, morphology, and composition. Substantial efforts have been made to relate the morphology to experimentally addressable properties of excitons confined in QDs [2]. The most easily accessible experimental property of a QD is its emission spectrum. In optical experiments, apart from the neutral exciton, one typically observes a family of lines corresponding to different (multiple or charged) excitonic complexes. The binding energies and line order of those excitonic complexes typically depend on nanostructure size, shape, and composition, which are the characteristic features of a given QD system [3]. In fact, this observation led to a recent proposal [3] that spectra of multiexcitonic complexes could be used to obtain (to reverse engineer) structural information such as QD size and shape. That procedure known as a "spectral bar coding" benefits from the fact that the excitonic line ordering seems to be the stable characteristic of a given system, even though the energy distances between emission lines are in fact very sensitive to different random realizations of an alloy [4].

In this work we study natural InAs/GaAs QDs (WLQDs) [5–8], which form in the wetting layer (WL) accompanying self-assembled InAs/GaAs QDs. The three-dimensional confinement of carriers in the WLQDs is related to potential fluctuations due to In composition fluctuations in the WL [7]. The WL disorder leads to the discrete structure of the WL-related emission. The nonclassical character of the optical emission related to excitons confined in the WLQDs was confirmed by the observation of biexciton-exciton emission cascades and the spectral antibunching [8].

We demonstrate that the spectral bar coding does not hold in the WLQDs. We show that not only the binding energy magnitudes but also the order of excitonic lines can vary within the dot ensemble, as recently observed in GaAs QDs [9] and small self-assembled InAs/GaAs QDs [10]. Presented calculations show that the observed variation can be explained in terms of the WLQD lattice randomness. It is shown that the randomness strongly affects the biexciton and positive trion binding energies, which is observed in our experiment.

II. MODEL

The WL composition fluctuations which correspond to our experiment are modeled by embedding an alloyed $In_xGa_{1-x}As$ WL into a bulklike GaAs matrix. The layer thickness is equal to four monolayers (∼1.2 nm). The indium content x in the layer area varies from 45% to 55% with a 1% step; that is, we consider 11 different compositions. For each composition eight different "distribution samples" are generated. Each sample is a different random realization (atomic arrangement) corresponding to the same average composition. For more details, see Fig. 1. For a given distribution sample the deviation of indium content from the nominal composition x is typically within 0.25%. This results in a family of $88 = 11 \times 8$ different systems used for computations.

*mzielin@fizyka.umk.pl

†katarzyna.golasa@fuw.edu.pl

 ©2015 American Physical Society

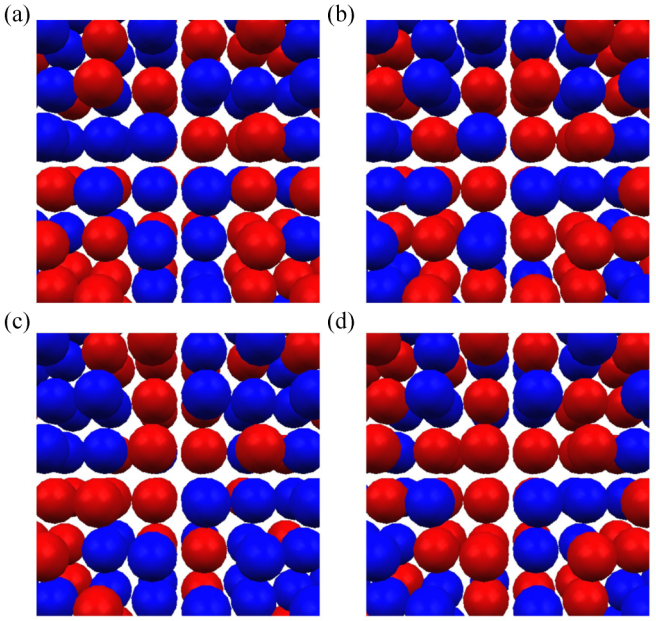

FIG. 1. (Color online) View of local atomic arrangement inside wetting-layer quantum dots demonstrating the effect of alloy fluctuations. Gallium atoms are shown as red (light gray) spheres, whereas indium atoms are shown as blue (dark gray) spheres. Common ions (arsenic atoms) as well as background atoms are not shown to improve clarity.(a)–(d) Different distribution samples correspond to different random realizations (local atomic arrangements), whereas the average composition (indium fraction) remains constant in all samples and equals ∼50%.

For comparison we have performed additional calculations for several systems of larger (∼1.5 nm) WL thickness. As we focus on the role of random fluctuations rather than a particular profile shape, in all cases we utilize a uniform composition profile.

Calculations involved three steps [11–21]: (i) the calculation of equilibrium positions of constituent atoms, (ii) the calculation of electron and hole single-particle (SP) states, and (iii) the inclusion of final-state interactions by defining an effective Hamiltonian of interacting excited quasiparticles, diagonalized using the configuration interaction (CI) method.

We use the approach with the relaxation of strain (calculation of atomic positions) included via the atomistic valence-force-field theory [22,23]. We model the external GaAs buffer as a cylinder 60 nm in diameter and 86 nm in height. The computational domain for the strain calculation has reached over 8×10^6 atoms, and its size guarantees convergence of the strain distribution [24]. With the equilibrium atomic positions known, the SP electronic structure is calculated. We use atomistic tight-binding theory [18] for electron and hole states with an $sp^3d^5s^*$ orbital model [18,25] and parameters taken from Ref. [25]. This model accounts for nearest-neighbor coupling, coupling between different parts of the Brillouin zone, and spin-orbit effects and includes strain due to lattice mismatch. The Coulomb and exchange integrals are calculated from the tight-binding eigenfunctions [17,26] as shown in Ref. [17], and the correlated excitonic states are calculated using the CI (exact diagonalization) approach [14,17]. By using a multiscale [24] approach the number of atoms for the SP calculation can be reduced. The tight-binding domain was modeled as a cylinder 22 nm in diameter and 15 nm in height with the WL in the center of the domain. Both the SP (tight-binding) and Coulomb matrix element calculation domains [24] contained $\sim 2 \times 10^5$ atoms. For the CI calculations we use all possible determinants constructed from the 12 lowest-energy electron and 12 lowest hole states (including spin).

III. EXPERIMENT

The sample investigated in this work was grown by molecular beam epitaxy using the In-flush technique [28]. It contained a single layer of self-assembled InAs/GaAs QDs, which were accompanied by the WL. Low-temperature microphotoluminescence (μ-PL) measurements were done using a cryostat. High spatial resolution was assured in the experiment by using a microscope objective. The diameter of the laser spot on the sample surface was lower than 1 μm. Two different lasers were employed to excite the sample: CWNd:YAG (532 nm) and light-emitting diode (LED) laser (650 nm). The μ-PL was resolved using a 0.5-m spectrometer with a CCD camera.

IV. RESULTS AND DISCUSSION

A. Transition energies

The μ-PL spectrum from the investigated structure comprises the emission from the GaAs barrier, self-assembled QDs [27], the WL, and the WLQDs. The WL-related emission (see Fig. 2) can be seen in the spectrum due to a relatively low density of self-assembled QDs [5]. The μ-PL spectrum in the energy range of the expected WL emission (1.42–1.44 eV) consists of several sharp lines suggesting its strongly disordered character. Moreover, in the energy range up to 10 meV below the WL-related emission a few discrete emission lines

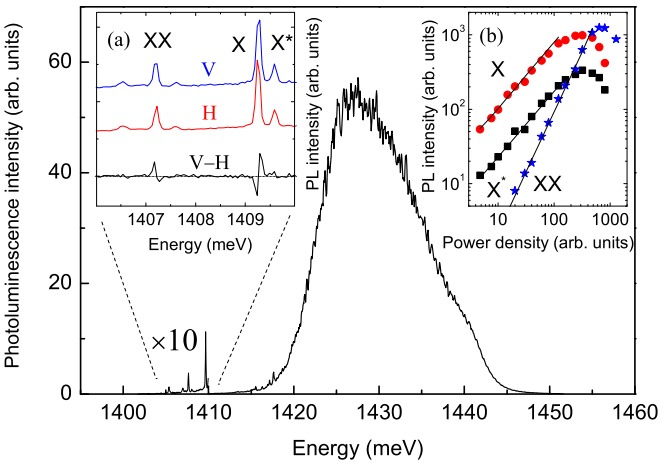

FIG. 2. (Color online) The low-temperature photoluminescence related to the recombination of carriers in the InAs/GaAs wetting layer. The results of polarization-sensitive measurements in the low-energy range of the spectrum are shown in inset (a). Photoluminescence spectra detected with vertical (V) and horizontal (H) linear polarization the difference spectrum (V-H) are presented. The power dependence of the observed features is shown in inset (b).

can be observed in the μ-PL spectra, which are related to the WLQDs.

At low excitation power density, usually, there are two emission lines in the spectrum related to the WLQDs: X and X^*. With the further increase of the excitation power, an additional emission line, XX, emerges in the spectrum at energy lower than E_X, the energy of the X emission line (see Fig. 2). A similar μ-PL spectral line shape can be found in several spots on the sample. The inspection of the CCD camera image confirms that all three emission lines originate from the same location on the sample. The WLQD-related emission is spatially anticorrelated with the emission from self-assembled QDs present in the structure (the latter dots are not addressed in this work). The average areal density of the WLQDs is 10^7 to 10^8 per square centimeter. Polarization-sensitive measurements confirm that the X emission line is split into two components linearly polarized in perpendicular directions [see Fig. 2, inset (a)]. The splitting results from the long-range component of the anisotropic electron-hole exchange interaction [29], and it supports the assignment of the X line to a neutral exciton in the WLQD. The splitting changes from dot to dot, and it is usually smaller than 20 μeV. This corresponds to the results of our theoretical calculations, which predict the bright-exciton splitting values to vary from 2 to 16 μeV and which show pronounced sample dependence. The strong dependence of the bright-exciton splitting on lattice fluctuations has already been theoretically reported for self-assembled and nanowire QDs [21,30].

In contrast, no splitting of the X^* emission line is observed, which is consistent with its attribution to a singlet trion, in which the exchange interaction is quenched.

The XX emission line consists of two components, which are linearly polarized in perpendicular directions (see Fig. 2). The splitting of XX is opposite to the neutral exciton splitting, which confirms the attribution of the XX emission line to the recombination of a neutral biexciton. Both X and X^* emission lines gain in intensity with increasing excitation power; however, the XX emission line dominates the spectrum excited with the highest power density.

It may also be noted that together with the X, XX, and X^* emission lines, several weaker lines can be observed, which may be due to other excitons (e.g., of the opposite charge or doubly charged). Those emission lines will not be considered in the further analysis as we define X^* as the strongest trion-related emission line.

B. Calculated vs experimental spectra

The energy range of the observed emission lines can be compared with the results of our calculations. The ground-state energy of a single neutral exciton calculated for all (88) considered distribution samples as discussed in Sec. II is presented in Fig. 3. The excitonic energy decreases from ~1430 to ~1385 meV with the increasing indium (low-band material) content in the WL, corresponding to a redshift of ~4.5 meV for each 1% of indium. Besides the apparent trend due to an average composition, there are noticeable variations due to random (alloy) fluctuations with a typical spread of ~10 meV. These fluctuations cannot be attributed only to the deviation from the nominal (average) composition of each

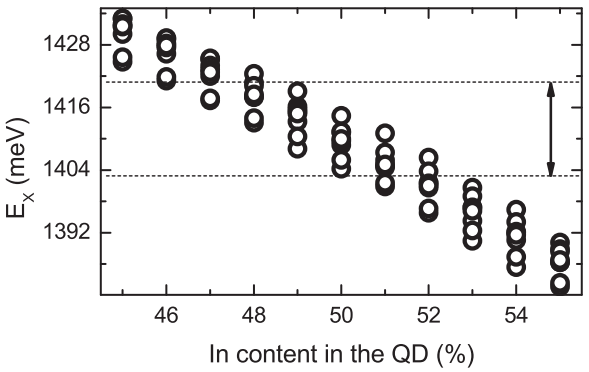

FIG. 3. Ground-state energies of neutral excitons confined in WLQDs calculated as a function of the average indium composition. Note the eight different random realizations for each average indium content. For comparison, dashed lines and arrows mark the spectral range of WLQD excitonic emission energies typically observed in the experiment.

sample (which is of the order of 0.25%, as approximately marked by the diameter of each circle in the plot), but rather, they are due to the effects of random alloy fluctuations between different distribution samples (random realizations). Therefore for two distribution samples of the same nominal composition the difference in excitonic energies can reach up to 10 meV.

We find that an average indium content within the 48% to 52% range matches excitonic energies observed in our experiment reasonably well.

Emission spectra of several excitonic complexes calculated for a few samples selected within a narrow spectral range (1404–1406 meV) of a neutral exciton's emission energy are presented in Fig. 4(a). Those spectra have been arranged with decreasing biexciton binding energy from top to bottom. It may be noticed that the random fluctuations not only change the binding energies of the excitonic complexes but can even lead to the transition of the positive trion binding energy from negative to positive values. This fact should be emphasized as reliable prediction of excitonic line order is of key importance for so-called inverse approaches [3], as discussed earlier.

This trend can also be traced in our experimental data. We have performed a systematic study of the relative energies of excitons, biexcitons, and trions, and a set of experimental spectra related to several WLQDs is presented in Fig. 4(b) as a function of the energy relative to E_X. Figure 4(b) shows that binding energies of excitonic complexes vary significantly from dot to dot. Figure 4(b) also shows that although the energies of XX and X^* substantially change, the trion energy E_{X^*} follows the biexciton energy E_{XX}, with an energy difference between the two of ~2–2.5 meV. As a result the order of the X, X^*, and XX lines can sometimes change.

The results of our experimental studies on more than 30 WLQDs in the structure are summarized in Fig. 5(a), in which the trion binding energies (defined as $E_{X^*} - E_X$) are plotted against the biexciton binding energy ($E_{XX} - E_X$). The correlation of the trion binding energy with the biexciton binding energy is apparent. The respective exciton emission energies E_X are presented in Fig. 5(b) as a function of the biexciton binding energy. It can be seen that the clear correlation of the trion binding energies with the biexciton

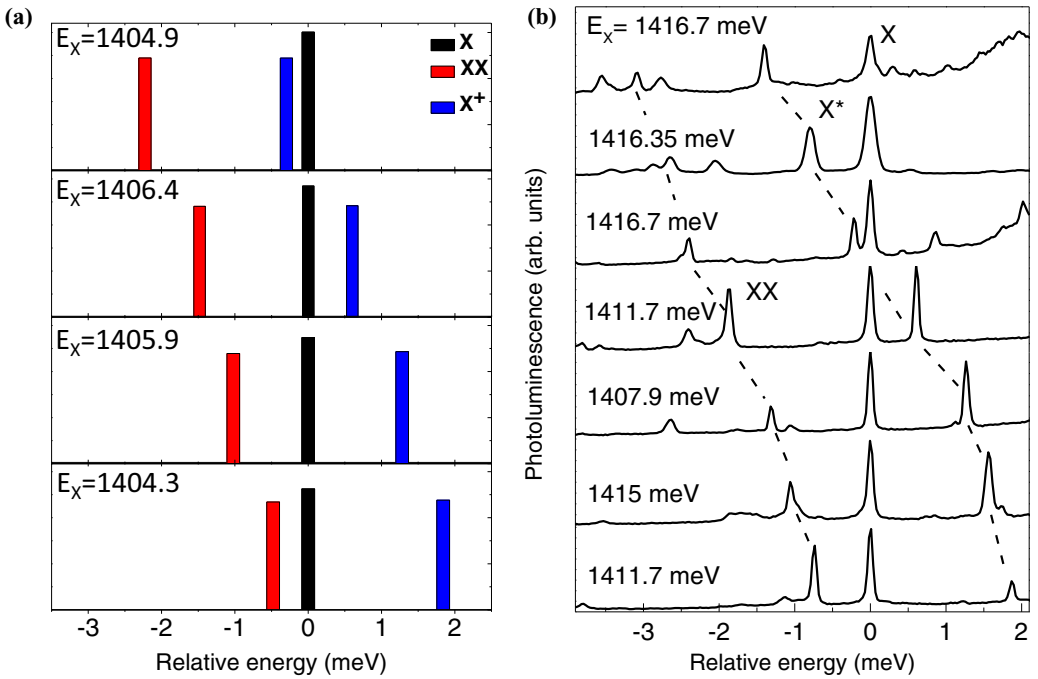

FIG. 4. (Color online) (a) The emission spectra calculated for several samples (see the text) with similar $E_X \approx 1405$ meV energy, which comprise emission lines due to the exciton (X), the biexciton (XX), and the positively charged exciton (X^+). (b) Photoluminescence spectra of several WLQDs with the neutral exciton (X), biexciton (XX), and the trion (X^*) emission lines. Measurements are taken at $T = 1.6$ K. Note the energy scale relative to the exciton emission energy, which is also shown for each spectrum.

binding energies [see Fig. 5(a)] exists despite a relatively large scatter in the exciton binding energies, which only weakly depend on the biexciton binding energies [see Fig. 5(b)].

Our data strongly support the attribution of the experimentally observed trion line X^* to the positively charged exciton X^+. This attribution based on the theoretically predicted evolution of the positive trion binding energy as a function of the biexciton binding energy is further supported by the presence of the expected background acceptor in the intentionally undoped GaAs layers [9]. Also its usual appearance in the spectrum is consistent with the larger probability for holes to be localized by potential fluctuations because their mass is higher than the mass of electrons [31].

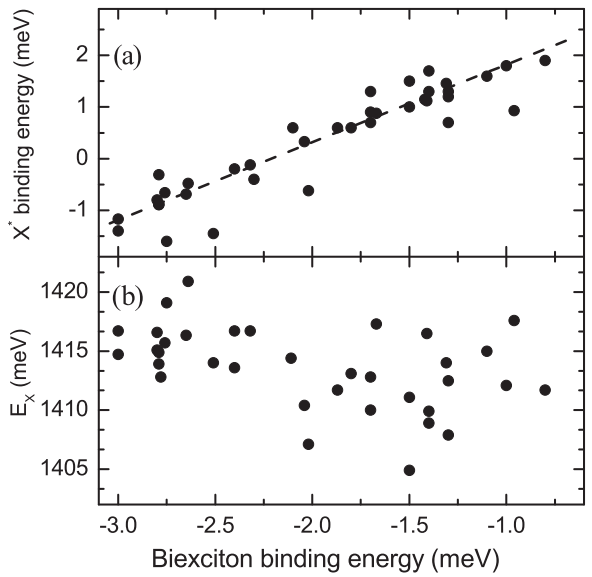

FIG. 5. (a) The trion binding energy and (b) the exciton emission energy, measured as a function of the biexciton binding energy. The line in (a) is a guide to the eye.

In the following, we address the apparent relation between the positive trion and biexciton emission energies. The calculated binding energies of the positively charged excitons X^+ are plotted with respect to the biexciton binding energy in Fig. 6(a). In the considered range of neutral exciton energies [1380–1430 meV; see Fig. 6(b)] the biexciton is bound, with the binding energy varying significantly from -0.5 to -2.5 meV depending on the distribution sample. The two dashed horizontal lines in Fig. 6(b) denote the spectral range used to create Fig. 4(a). The biexciton binding energy is thus a very sensitive function of the lattice randomness with nearly flat dependence on the exciton energy. Similar 2 meV uncertainty in the binding energy due to lattice randomness can be observed for the positive trions. Large variations for different random realizations lead in some cases to a transition from the positive to negative (-0.5 meV) binding energies of the positive trions, therefore reversing the order of excitonic lines as observed in the experiment. One may again notice that although the energies of multiexcitonic complexes can vary significantly with respect to the neutral exciton energy, there is an apparent alignment of the XX and X^+ lines with a fixed separation between those lines equal to $\sim$2 meV [see Fig. 6(a) and compare with Fig. 5(a)]. It should be noted that the XX and X^+ spacing close to 2 meV is present not only for several "cherry-picked" samples but also for all systems considered in our calculations.

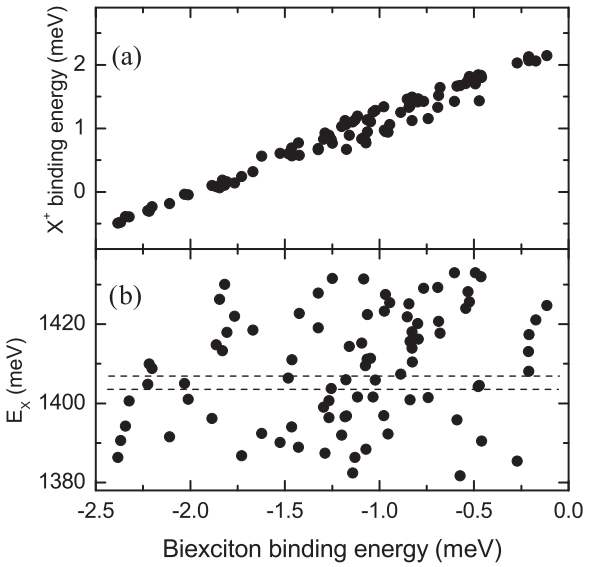

FIG. 6. (a) The binding energy of a positively charged exciton (X^+) and (b) the exciton emission energy calculated for all distribution samples considered in the calculation.

C. Binding energies

In order to analyze the physical origin of the apparent correlation between the biexciton and positive trion binding energies one should first note that excitonic binding energies must be calculated using the full many-body approach [32,33]:

$$\begin{aligned} XX_{\mathrm{CI}} &\equiv E_{XX} - E_X = J^{ee} + J^{hh} - 2J^{eh} - \Delta(XX) \\ &= XX_{\mathrm{HF}} - \Delta(XX), \\ X^+_{\mathrm{CI}} &\equiv E_{X^+} - E_X = J^{hh} - J^{eh} - \Delta(X^+) \\ &= X^+_{\mathrm{HF}} - \Delta(X^+), \\ X^-_{\mathrm{CI}} &\equiv E_{X^-} - E_X = J^{ee} - J^{eh} - \Delta(X^-) \\ &= X^-_{\mathrm{HF}} - \Delta(X^-), \end{aligned} \tag{1}$$

with electron-electron (J^{ee}), hole-hole (J^{hh}), and electron-hole (J^{eh}) Coulomb integrals calculated for an electron and a hole occupying their ground single-particle states. The important correction due to correlation effects Δ can be attributed to the effects of configuration mixing with higher-lying states. In the Hartree-Fock (HF) or the perturbation theory approximation $\Delta = 0$. Realistic values of binding energies ($\Delta \neq 0$) can be calculated using the full CI method [32,33]. Figure 7 shows binding energies calculated for the same family of four samples as that presented in Fig. 4(a), obtained using a full CI approach [Fig. 7(a)] and with a perturbative (HF approximation) approach [Fig. 7(b)]. As shown in Fig. 7, the absolute value of the binding energy must be calculated using the many-body approach, with the important correction due to correlations (Δ) reaching up to 4 meV for some of the excitonic complexes.

Such a large correction due to correlation effects can be attributed to a strong mixing of closely spaced (typically

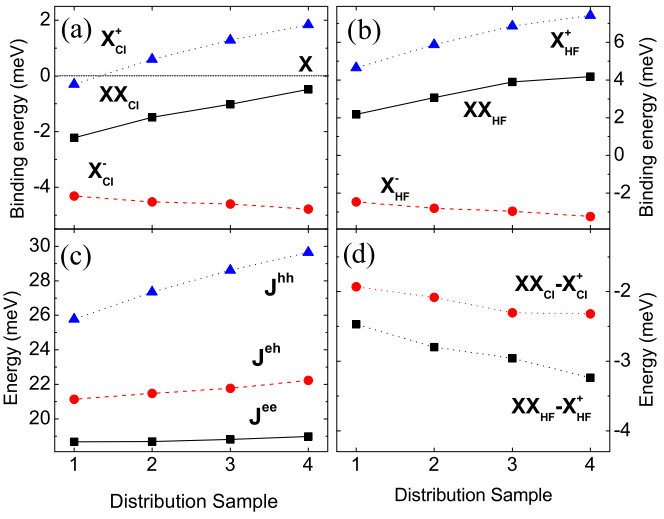

FIG. 7. (Color online) The biexciton (XX), the positively (X^+) and negatively (X^-) charged binding energies calculated using (a) the configuration interaction (CI) approach and (b) the perturbative approach (Hartree-Fock approximation, HF). (c) Electron-electron (J^{ee}), electron-hole (J^{eh}), and hole-hole (J^{hh}) Coulomb integrals for electrons and holes occupying their ground states. (d) The biexciton (XX) and the positively charged (X^+) exciton line spacings calculated using the CI and HF approaches. The results shown here were obtained for four different random realizations (samples) identical to those in Fig. 4(a) (with up-down ordering replaced with 1, 2, 3, and 4). Lines are guides to the eye.

2 meV; not shown here), excited (the WL quasicontinuum), SP hole states.

The energy spacing of excited electron levels is much larger, with a typical value of ~30 meV (not shown here). However, for both types of carriers, due to the large degree of alloying and spatial delocalization, it is hard to unambiguously classify excited SP states as having purely WLQD (fluctuation) or WL character. Only the ground electron and hole states can be explicitly classified as WLQD states. This is due to their good spectral separation from the rest of the WL continuum, rather than the particular spatial localization.

Returning to the subject of binding energies, irrespective of the correlation effects and as seen in Fig. 7(b), the quantitative trend for different distribution samples can be understood at the level of the HF approximation and by analyzing several electron-hole Coulomb integrals [J^{ee}, J^{eh}, and J^{hh}; shown in Fig. 7(c)]. The electron-electron repulsion integral does not vary significantly between different random realizations, with less than 1 meV difference between them. This is a hallmark of a large electron delocalization and a small susceptibility to (local) random lattice fluctuations. Moreover the electron states are built predominately from s-type atomic orbitals, and they are affected (in the Bir-Pikus formalism [34]) by only the hydrostatic component of strain. The hydrostatic strain leads predominantly to a simple energetic upward shift due to bond-length contraction in the strained system.

Holes are typically more localized than electrons due to their larger effective mass. They are also built from directional p-type orbitals, and their confining potential is strongly affected by the highly spatially variable biaxial strain

[19]. As a result the hole-hole repulsion Coulomb integral depends significantly on alloying effects, and it can scatter within as much as 4 meV for different random realizations. In contrast, the electron-electron and the electron-hole Coulomb integrals are, to a large degree, unaffected by the sample (local) effects.

Using Eq. (1), one can write explicitly

$$E_{XX} - E_{X^+} \equiv XX_{\mathrm{CI}} - X^+_{\mathrm{CI}} = J^{ee} - J^{eh} - \Delta(XX - X^+),$$
$$XX_{\mathrm{HF}} - X^+_{\mathrm{HF}} = J^{ee} - J^{eh}. \quad (2)$$

The "fixed" line spacing of the biexciton and the positive trion is governed at the level of the perturbation theory by a small variation in $J^{ee} - J^{eh}$ between different random distribution samples. On the other hand, from Eq. (1) one has $X^+_{\mathrm{HF}} = J^{hh} - J^{eh}$, and thus large J^{hh} changes are responsible for the transition from the negative to positive binding energy of the positive trion. Finally, as discussed above, although correlation effects play a fundamental role for the WLQDs [Fig. 7(d)], the variation of the correction due to correlations $\Delta(XX - X^+)$ is below 0.5 meV for different random realizations. Although $\Delta(XX - X^+)$ plays a smaller role, its variation between samples further stabilizes the $XX - X^+$ energy spacing.

V. CONCLUSIONS

In conclusion we have studied the properties of excitons confined in natural QDs formed in the InA/GaAs WL. Theoretical calculations showed that the biexciton binding energy in the investigated dots was a very sensitive function of the lattice randomness with nearly flat dependence on the exciton energy. The large variation in different random realizations of the QD structure was shown to lead in some cases to reversing the order of excitonic lines. The calculations are supported by our experimental results. Substantial variation of the binding energies of the biexciton and the trion was observed, with the transition from the negative to positive binding energy of the trion, which reverses the order of excitonic lines, as predicted theoretically. The analysis of experimental data within the presented theory allowed us to identify the observed trion as a positively charged exciton.

ACKNOWLEDGMENTS

The support from the Polish National Science Center based on Decisions DEC-2011/01/D/ST3/03415 (M.Z) as well as DEC-2013/08/T/ST3/00665 and DEC-2013/09/N/ST3/04237 (M.R.M) is acknowledged. The work was supported in part by the EuroMagNET II consortium under EU Contract No. 228043.

[1] *Optics of Quantum Dots and Wires*, edited by G. W. Bryant and G. Solomon (Artech House, Boston, 2005).
[2] J.-W. Luo and A. Zunger, Phys. Rev. B **84**, 235317 (2011).
[3] V. Mlinar, M. Bozkurt, J. M. Ulloa, M. Ediger, G. Bester, A. Badolato, P. M. Koenraad, R. J. Warburton, and A. Zunger, Phys. Rev. B **80**, 165425 (2009).
[4] V. Mlinar and A. Zunger, Phys. Rev. B **80**, 205311 (2009).
[5] A. Babinski, J. Borysiuk, S. Kret, M. Czyz, A. Golnik, S. Raymond, and Z. R. Wasilewski, Appl. Phys. Lett. **92**, 171104 (2008).
[6] A. Babinski, M. Czyz, J. Borysiuk, S. Kret, A. Golnik, S. Raymond, J. Lapointe, and Z. R. Wasilewski, Acta Phys. Pol. A **114**, 1055 (2008).
[7] M. Hugues, M. Teisseire, J.-M. Chauveau, B. Vinter, B. Damilano, J.-Y. Duboz, and J. Massies, Phys. Rev. B **76**, 075335 (2007).
[8] T. Kazimierczuk, A. Golnik, P. Kossacki, J. A. Gaj, Z. R. Wasilewski, and A. Babinski, Phys. Rev. B **84**, 115325 (2011).
[9] M. Abbarchi, T. Kuroda, T. Mano, K. Sakoda, C. A. Mastrandrea, A. Vinatteri, M. Gurioli, and T. Tsuchiya, Phys. Rev. B **82**, 201301 (2010).
[10] M.-F. Tsai, H. Lin, C.-H. Lin, S.-D. Lin, S.-Y. Wang, M.-C. Lo, S.-J. Cheng, M.-C. Lee, and W.-H. Chang, Phys. Rev. Lett. **101**, 267402 (2008).
[11] L. He and A. Zunger, Phys. Rev. B **73**, 115324 (2006).
[12] A. J. Williamson, L. W. Wang, and A. Zunger, Phys. Rev. B **62**, 12963 (2000).
[13] A. Schliwa, M. Winkelnkemper, and D. Bimberg, Phys. Rev. B **76**, 205324 (2007).
[14] W. Sheng, S.-J. Cheng, and P. Hawrylak, Phys. Rev. B **71**, 035316 (2005).
[15] M. Korkusiński, M. Zieliński, and P. Hawrylak, J. Appl. Phys. **105**, 122406 (2009).
[16] G. W. Bryant, M. Zielinski, N. Malkova, J. Sims, W. Jaskolski, and J. Aizpurua, Phys. Rev. B. **84**, 235412 (2011).
[17] M. Zielinski, M. Korkusinski, and P. Hawrylak, Phys. Rev. B **81**, 085301 (2010).
[18] M. Zielinski, Phys. Rev. B **86**, 115424 (2012).
[19] M. Zielinski, J. Phys. Condens. Matter. **25**, 465301 (2013).
[20] M. Zielinski, Phys. Rev. B **88**, 115424 (2013).
[21] M. Zielinski, Phys. Rev. B **88**, 155319 (2013).
[22] P. N. Keating, Phys. Rev. **145**, 637 (1966); R. M. Martin, Phys. Rev. B **1**, 4005 (1970).
[23] Y. M. Niquet, Phys. Rev. B **74**, 155304 (2006).
[24] M. Zielinski, Acta Phys. Pol. A **122**, 312 (2012).
[25] J. M. Jancu, R. Scholz, F. Beltram, and F. Bassani, Phys. Rev. B **57**, 6493 (1998).
[26] S. Schulz, S. Schumacher, and G. Czycholl, Phys. Rev. B **73**, 245327 (2006).
[27] A. Babinski, G. Ortner, S. Raymond, M. Potemski, M. Bayer, W. Sheng, P. Hawrylak, Z. Wasilewski, S. Fafard, and A. Forchel, Phys. Rev. B **74**, 075310 (2006).
[28] Z. R. Wasilewski, S. Fafard, and J. P. McCaffrey, J. Cryst. Growth **201–202**, 1131 (1999).
[29] D. Gammon, E. S. Snow, B. V. Shanabrook, D. S. Katzer, and D. Park, Phys. Rev. Lett. **76**, 3005 (1996).
[30] R. Singhm and G. Bester, Phys. Rev. Lett. **104**, 196803 (2010).
[31] E. S. Moskalenko, M. Larsson, W. V. Schoenfeld, P. M. Petroff, and P. O. Holtz, Phys. Rev. B **73**, 155336 (2006).
[32] A. Wojs, P. Hawrylak, S. Fafard, and L. Jacak, Phys. Rev. B **54**, 5604 (1996).
[33] M. Zielinski, Nanoscale Res. Lett. **7**, 265 (2012).
[34] G. L. Bir and G. E. Pikus, *Symmetry and Strain-Induced Effects in Semiconductors* (Wiley, New York, 1975).